Dynamics of dielectric barrier discharges in coplanar arrangements

INSTITUTE OF PHYSICS PUBLISHING JOURNAL OF PHYSICS D: APPLIED PHYSICS
J. Phys. D: Appl. Phys. **37** (2004) 2082–2092 PII: S0022-3727(04)77966-8

Dynamics of dielectric barrier discharges in coplanar arrangements

Valentin I Gibalov[1] **and Gerhard J Pietsch**[2]

[1] Department of Chemistry, Moscow State University, Leninsky Gory, 119899 Moscow, Russia
[2] Gas Discharge Engineering, RWTH Aachen University, Schinkelstr. 2, 52056 Aachen, Germany

E-mail: pietsch@ifht.rwth-aachen.de and gibalov@valentin.chem.msu.su

Received 18 March 2004
Published 14 July 2004
Online at stacks.iop.org/JPhysD/37/2082
doi:10.1088/0022-3727/37/15/006

Abstract
The development of a discharge channel in coplanar dielectric barrier arrangements is investigated numerically. Its behaviour in oxygen, like the spatial and temporal distributions of the field strength, charged and neutral particles and energy density, is described in detail. It is found that the streamer development is mainly determined by photoemission. A cathode layer appears near the position where the cathode directed streamer touches the dielectric surface. Secondary electron emission by ion collisions becomes significant and the parameters of the cathode layer are near those of a normal glow discharge. The charge transfer and energy release happen in the conductive channel of the discharge, which appears on the dielectric surface as a result of the cathode streamer development. The field strength in the conductive channel is nearly constant and about 70–100 Td in oxygen and air.

(Some figures in this article are in colour only in the electronic version)

1. Introduction

Recent developments have shown that a broad range of applications of non-thermal plasmas, like backlight sources for liquid crystal displays, plasma screens, surface treatment and chemical synthesis, exists. For example, economic ozone production in large amounts is only possible using non-equilibrium discharges. The most frequently used type of discharge in all these applications is the dielectric barrier discharge (DBD). DBD arrangements are characterized by a dielectric layer covering at least one of the electrodes.

Apart from the conventional DBD arrangement with a gas gap (volume discharge, VD), there exist devices where the DBD develops on a dielectric surface. If a dielectric layer covers (a) pair(s) of long electrodes placed on a dielectric plate, discharge channels develop along and on/above the dielectric layer between each pair of electrodes (figure 1). In general the electrode gaps of coplanar discharge (CD) arrangements are of the order of 100 μm, and the thickness of the dielectric layer is about 10–60 μm, depending on the application.

The most remarkable application of CDs is the plasma display panel (PDP). The use of CDs for ozone synthesis is a relatively recent but prospective application. The behaviour of barrier discharges in CD arrangements and electronegative gases (as in ozone synthesis from oxygen) differs from that in rare gases (as in PDPs). A comparison of the discharge dynamics in the two cases allows a better understanding of the basic properties of CDs and broadens the knowledge on barrier discharges.

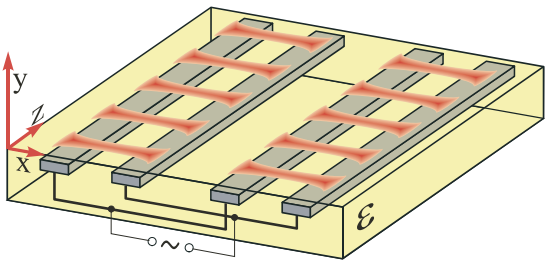

Figure 1. Sketch of a CD arrangement.

A CCD picture of a CD in air is presented in figure 2. The discharge consists of distinct parallel discharge channels that originate and terminate at the locations of the electrodes

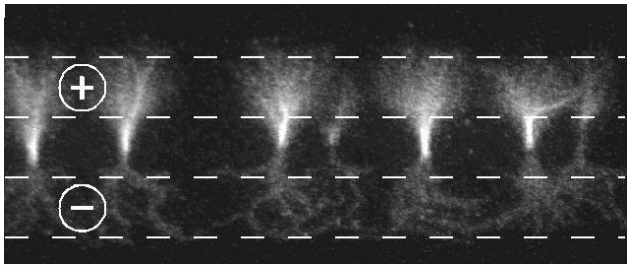

Figure 2. Top view of a CD in atmospheric air. The location of the electrodes is marked with dotted lines, the inter-electrode distance is 2 mm and the exposure time half a cycle of the applied voltage [1].

on the dielectric surface. The filament structure is common for barrier discharges in gas gaps and on surfaces. The average distance between the channels is of the order of the inter-electrode distance. The channels seem to appear simultaneously and develop rather independently of their neighbours. The preceding channels influence the succeeding ones by surface charges left on the dielectric surface.

There are plenty of articles dealing with experimental investigation of CDs as well as their numerical modelling. A majority of them address PDPs. However, there are only a small number on experimental results [1, 2] and modelling aspects of ozone synthesis in CD arrangements [3–9].

The aim of this article is to summarize recent results of numerical investigations of the discharge behaviour in coplanar arrangements. The most important goal of the modelling is to obtain data concerning the discharge dynamics in CDs in general and in particular considering electronegative gases of atmospheric pressure. One of the most important aspects of the dynamics is the energy transfer from the electric field to charged particles and further on to internal states of atoms and molecules. Ozone synthesis was chosen as a convenient application for this purpose, and therefore most of the results apply to this.

In this contribution the main focus is on the description of the dynamics of a single discharge channel, while in a succeeding paper the properties of a multitude of channels (of a whole CD device) are considered [10].

2. Numerical model

Modelling of DBDs means calculation of the temporal behaviour of the electric field distribution in the discharge region simultaneously with the dynamics of charged particles. The width of the channels is small compared with the inter-channel distance (figure 2). Decreasing the electrode gap to 100 μm or less than the inter-channel distance is practically indentical. That is why a two-dimensional approach is chosen, which allows us to obtain reliable results with relatively little effort (technical difficulties). In this case the discharge is taken as being uniform in one dimension (along the length of the electrodes, z-coordinate in figure 1). If the channel structure of the discharge is of importance (e.g. to determine the current and energy per unit electrode length), the width of the discharge channel can be taken into account.

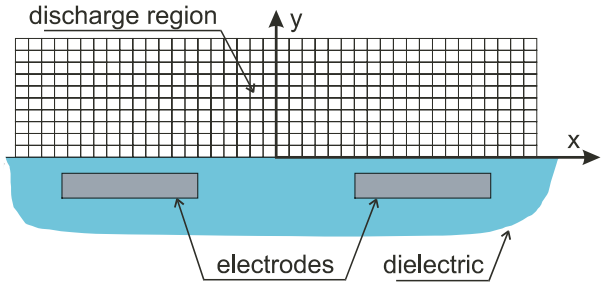

Figure 3. Sketch of the discharge region of the CD arrangement.

A sketch of the discharge region (with integration grid) is presented in figure 3. Two-dimensional simulations are carried out in the xy-plane.

2.1. Transport equations, initial and boundary conditions

In general the dynamics of charged as well as neutral particle densities is described by a system of Boltzmann equations. A direct solution is time consuming [11–15]. As the results do not differ significantly from those obtained using the local field approximation (LFA) [11, 16–22], the LFA approach is used here. The system of continuity equations of this approach, describing the spatial and temporal distribution of all particles, consists of

$$\frac{\partial n_i}{\partial t} + \operatorname{div}(\vec{j}_i) = S_i, \tag{1}$$

$$\vec{j}_i = D_i \cdot \operatorname{grad} n_i + \vec{v}_i \cdot n_i, \tag{2}$$

where n_i, $\vec{j}_i$, S_i, D_i and $\vec{v}_i$ are the number density of charged particles, the current density, the source term, the diffusion coefficient and the drift velocity of the ith component of the plasma. The source term includes, e.g. ionization, attachment and detachment processes.

In order to solve this system the initial and boundary conditions must be fixed. There are two types of boundaries, at the dielectric surface, and those that limit the integration region in the gas space (external boundaries). The dielectric surface is taken as adsorbing particles and apart from this as a source of secondary electrons. They are released by photon and ion impact processes. The resulting flux of secondary electrons is given by

$$n_e \cdot v_e = \gamma_+ \cdot n_+ \cdot v_+ + \gamma_{ph} \cdot \phi. \tag{3}$$

The photon flux density, ϕ, on the surface is taken to be proportional to the ionization rate and can be determined by integration over the whole discharge volume. The emission coefficients (γ_+ and γ_{ph}) are varied during modelling from 0.001 to 0.3.

The external boundaries are open; particles reaching this boundary may leave the integration region.

The following initial conditions are used:

(a) initial electron–ion pairs (seed electrons) are homogeneously distributed in a layer near the dielectric surface,
(b) the net charge in the gas region is zero,
(c) the initial charge density on the dielectric surface is zero; if a set of discharges is considered, the surface charge density is determined by the residual charges from all previous discharges.

The drift velocities of the charged particles and the ionization as well as the attachment–detachment coefficients as functions of E/n are taken from [27]. The functions are introduced in the model as tables. Intermediate values are taken from linear approximation.

The continuity equations are solved using an explicit method. To compensate or limit the numerical diffusion, a *flux-correction technique* algorithm [23–25] has been applied.

2.2. Field calculation

As the CD arrangement under consideration consists of two regions with different permittivity (gas volume and dielectric plate), the Poisson equation must be solved in both to find the field configuration:

$$\mathrm{div}(\vec{E}) = \frac{1}{\varepsilon_0 \cdot \varepsilon_i} \cdot \rho_i, \tag{4}$$

where ε_i is the relative permittivity and ρ_i the total charge density of the corresponding region. To solve the Poisson equation the potential on the dielectric surface and the external boundaries of the integration region must be known.

In order to determine the boundary potentials, the image charge method has been applied. In general the potential at any point of the integration region is defined by charges on the surface of the conductive electrodes, by charges on the dielectric surface and by space charges in the discharge region. The dielectric can be excluded from the considerations if each existing charge has an image charge. The position, as well as the value, of the image charge is connected with its origin by the known relations of the tangential and normal components of the field strength at the dielectric boundary. The entirety of charges (surface charges of the conductive electrodes, surface charges on the dielectric surface and the space charges in the discharge region together with their image charges) enables the correct determination of the potential distribution on the boundaries, especially on the dielectric surface. The procedure for handling the image charge and charge simulation methods simultaneously is described, e.g. in [7, 26].

The positions of the charges of the conductive electrodes and those of their images are fixed. Their values are determined by the actual potential at the electrodes at any time of the discharge process.

The discharge arrangement is an element of the electrical circuit, which consists of several impedances. In general the voltage at the electrodes is not constant during discharge development. To obtain the voltage a system of circuit equations must be solved together with the simulation of the discharge development. 'Discharge simulation' means solving the system of transport equations (1) and (2) on several ten thousands of grid points. A few additional equations describing the circuit should not complicate the procedure. There are two asymptotic approaches, which allows separate solution of the two systems of equations.

If the circuit includes a large impedance, the circuit will not be able to supply the discharge arrangement during the fast breakdown process. It behaves as though it is disconnected from the external power supply. At this condition the charge at the electrodes remains unchanged during breakdown (Q = const); however, the voltage at the electrodes will decrease.

If on the other hand the circuit impedance is nearly zero, the power supply is able to support the discharge current during the breakdown process. Under this condition the voltage at the electrodes remains unchanged (V = const).

In reality the conditions are in between these asymptotic cases. Both approaches are used.

3. Discharge development

The parameters of the discharge arrangement under consideration are as follows: the electrode gap and thickness of the dielectric layer above the electrodes are varied in the range between 80 μm and 650 μm and between 20 μm and 200 μm, respectively. The width of the electrodes is between 60 and 150 μm, and the relative permittivity of the dielectric between 5 and 15 μm. If not otherwise mentioned, the following values are used:

(a) thickness of dielectric plate 1 mm,
(b) thickness of dielectric layer above electrodes 55 μm,
(c) thickness of electrodes 5 μm,
(d) width of electrodes 120 μm,
(e) gap between electrodes 80 μm,
(f) relative permittivity 10,
(g) oxygen of 1.7 bar pressure.

3.1. Electric field distribution

The initial field strength distribution above the dielectric surface resulting from a voltage of 2100 V applied to the electrodes is presented in figure 4. The tangential field strength component reaches its maximum between the electrodes. The normal field strength component is positive at the location of the positive electrode (left one) and negative at the earthed one. This means electrons drift from the right to the left electrode.

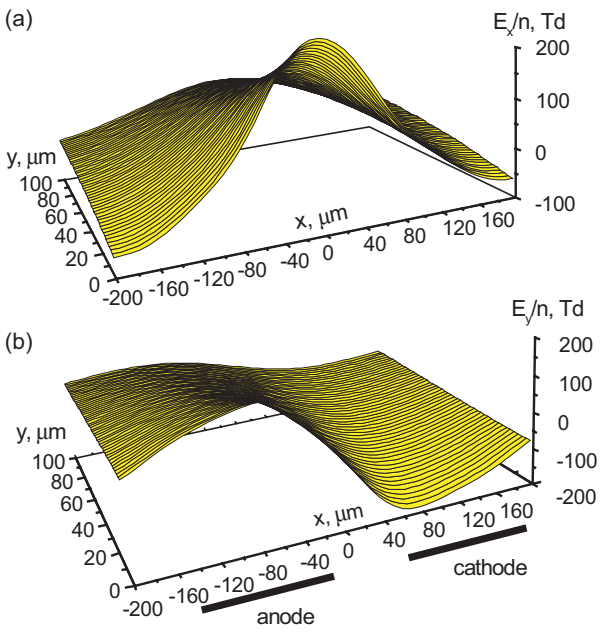

Figure 4. Initial field strength distribution above the dielectric surface: (*a*) tangential component and (*b*) normal component (2100 V, 1.7 bar oxygen).

To trigger the discharge, seed electrons are injected in the discharge region (figure 3). These electrons move towards the anode. Due to their multiplication by collision processes their number density rises and a field distortion appears at a certain level of the charged particle density (figure 5, 1.3 ns). Its amplitude is 1.5 times larger than the maximum of the initial field strength. In a few nanoseconds this maximum propagates along the cathode and passes a distance of 50–70 μm (figure 5). The propagation velocity of this cathode-directed streamer is of the order of 10^7 cm s^{-1}. This value is of the order of the electron drift velocity. The streamer moves in the direction opposite to the electron flux (cathode-directed streamer).

Above the anode a side maximum of the field strength appears as well (figure 5, 1.3 ns). This looks like an anode-directed streamer, which in contrast to the main one propagates in the direction of the electron flux (to the left side). The thickness of both streamers is about 20–30 μm (figures 5 and 6). The simultaneous movement of both streamers smoothes the initial field distribution (figure 6). A plateau of the field strength appears between the streamer heads in the range between about -40 and +40 μm (see figures 5 and 6).

The tangential field strength distribution between the electrodes becomes more level. It reaches a level of 50–70 Td (figure 6). During the fast movement of the streamers (compare $t = 1.3$ ns with $t = 3.2$ ns of figure 5) the region between the two maxima increases and reaches a length of about 150–200 μm.

The distribution of the normal component of the field strength shows some peculiarities. At the location of the cathode, a deep field strength minimum appears (on the right side of figure 6). Its amplitude reaches a level of about -900 Td. The parameters of this structure, e.g. the values of field strength and of current density of about 10–20 A cm^{-2}, are not far from those of the cathode layer of a normal glow discharge. The thickness of this structure (cathode layer) is 20 μm, and its width is 50–60 μm at 1.3 ns. It subsequently increases up to 150 μm (figure 6, 23.9 ns). The cathode layer becomes an effective source of secondary electrons and by this supports the propagation of both streamers. Photoemission is less important after cathode layer formation.

The electrons reach the dielectric surface at the location of the anode. The normal component of the field strength becomes zero here (figure 6); however, electrons move farther and finally reach the far edge of the anode position during the extinction phase.

During the extinction phase the electron flux decreases and the field strength in the cathode layer collapses too due to an accumulation of positive charges on the dielectric surface. The width of the cathode layer continues to broaden and nearly reaches the far edge of the electrode position at the end of the extinction phase.

The duration of the discharge phase, where the streamer develops and the cathode layer is built up (electron phase), is about 5 ns under the given conditions. During the extinction phase, which follows the electron phase, the intensity of all discharge processes decreases further on owing to a significant drop in the mean field strength. From this point on the ion movement determines the discharge behaviour and causes a further smoothing of the field strength distribution.

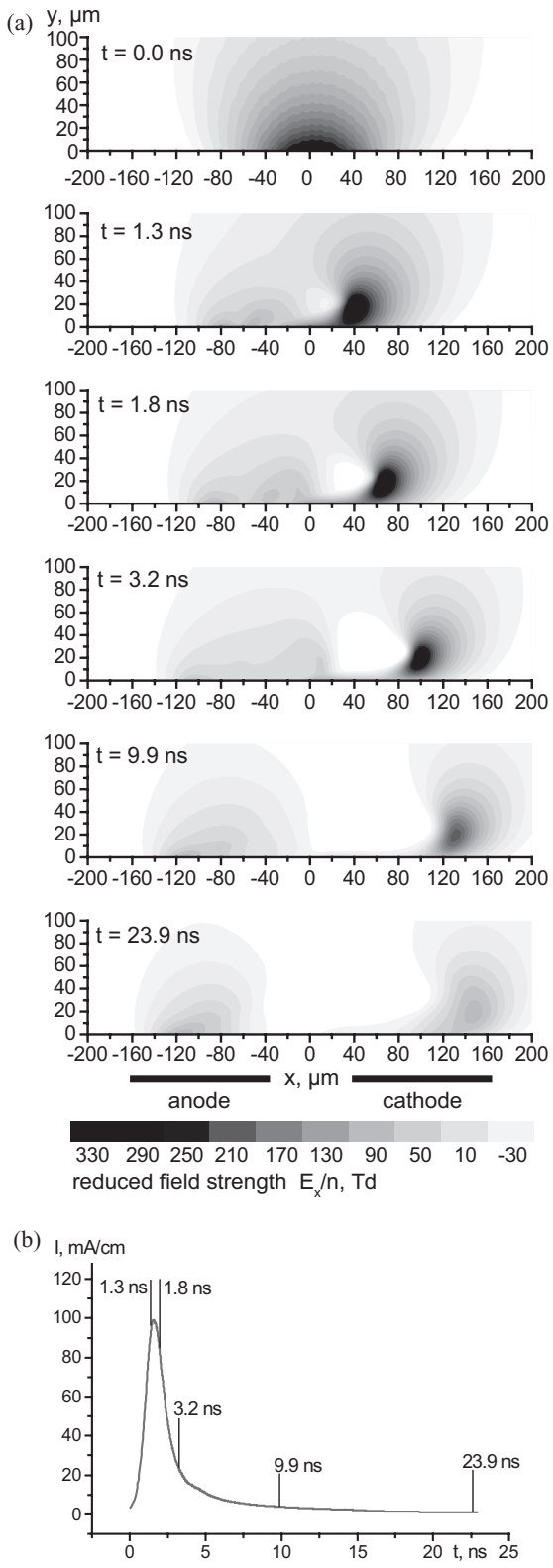

Figure 5. (*a*) Temporal development of the tangential field strength distribution (2100 V, 1.7 bar oxygen) and (*b*) the corresponding current pulse with marked time steps.

3.2. Dynamics of charged particles

The charge transfer causes a highly conductive discharge channel with maximum electron densities of 10^{14} cm^{-3} and

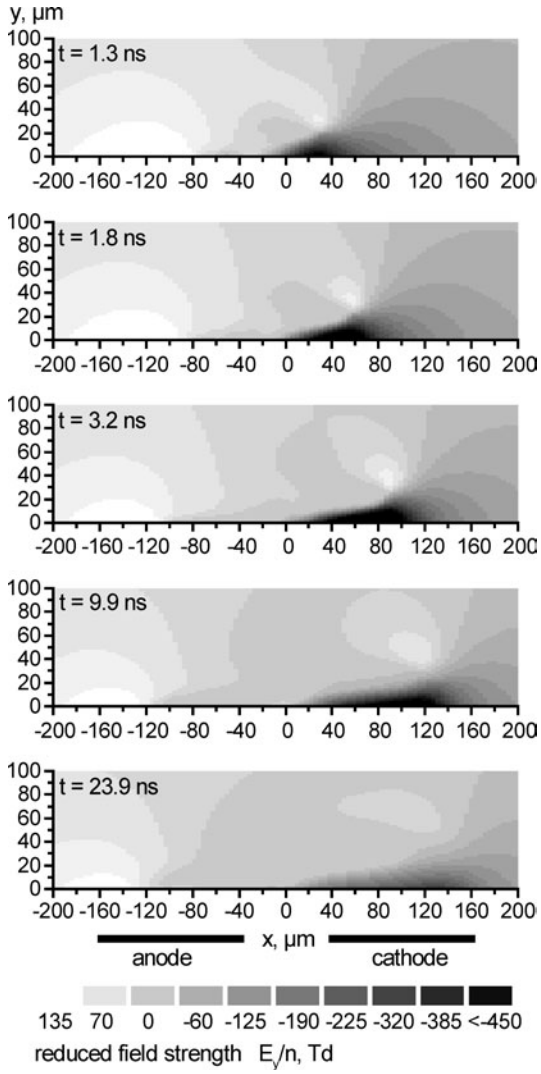

Figure 6. Distribution of the normal field strength component at an early stage of the discharge development (on the top) and during the extinction phase (on the bottom).

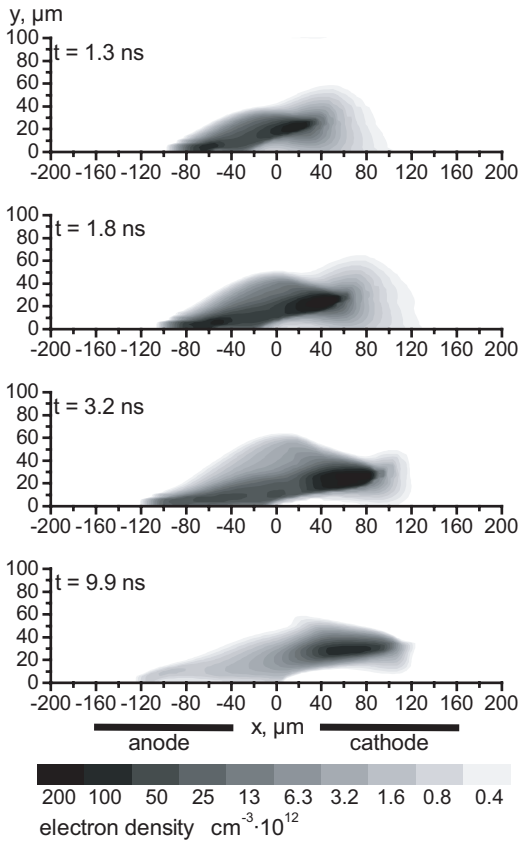

Figure 7. Temporal development of the electron density distribution.

more behind the streamer head (figure 7). The channel develops at the location of the field strength plateau (compare figures 5 and 6 with figure 7). It lengthens with time and finally reaches 125 μm. Its thickness is about 20–25 μm.

The density of any charged particle in the channel increases during the steep rise in the current pulse. Later on the amount of positive and negative charges in the discharge region reaches maximum values and then decreases continuously during the extinction phase.

The net charge in the channel is zero, and the channel is quasi-neutral. In the region before the cathode (cathode layer) the net charge is positive as in the situation in glow discharges. Near the anode at the opposite side of the channel the total charge density is negative. That is why the region with net charge zero is situated between two charged regions with opposite polarity, which reduces the external field strength.

A kind of equilibrium between the density of the charged particles and the mean field strength follows the streamer head. This equilibrium appears in the conductive channel with high electron density. Here the electron production rate is balanced by the attachment rate and the movement of electrons. If the electron density drops at a certain location of the channel, the field strength will rise immediately. This rise will increase the ionization rate and decrease attachment processes so that the electron density will increase as well and vice versa. This is the reason why the field strength does not drop to zero but is about 70–100 Td (in electronegative gases). This value of the field strength is close to that given at the crossing point of the curves of the attachment and ionization coefficient over field strength.

The surface charge density increases continuously (figure 8). In the electron phase mainly electrons are collected on the dielectric surface (in the region from -150 to 0 μm in figure 8). The surface charge density increases up to a certain level (60–70 nC cm^{-2}) at which the normal field strength component becomes zero. The succeeding electrons move over the surface and reach the dielectric surface further away, increasing the size of the charged spot (the region with zero normal field strength component in figure 6). During the extinction and ion phases the ion movement smoothes the surface charge distribution and makes it more symmetric (figure 8).

Looking at the discharge development, secondary electrons are produced by ion and photon impact on the surface. If only ion impact is included in the model, the timescale of the discharge development is determined by the ion drift velocity, and the process develops rather slowly. The distribution of the surface charge is comparably narrow in this case. The charge density does not exceed a level of 15–30 nC cm^{-2}. However, if

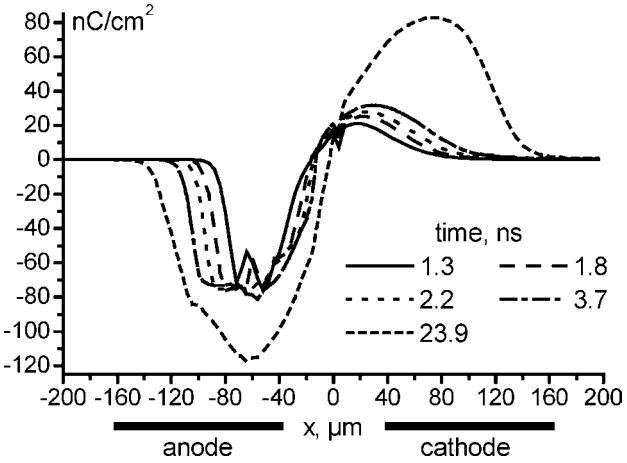

Figure 8. Distribution of surface charge density during discharge development.

photoemission is added, the charge transfer occurs much faster, and the value of the transferred charge is 5–6 times higher, with corresponding consequences for the charge density.

3.3. Ion phase

After the end of the electron phase the number density of electrons drops several orders of magnitude in the extinction phase. The charges collected on the dielectric surface decrease the field strength in the discharge region. Together with this, excitation and dissociation processes are terminated. A considerable amount of ions of both polarities are left in the discharge region. The drift of these particles (ion phase) decreases the electric field further and enhances the surface charges. After the ion phase the initial conditions for the next discharge pulse are given. Another effect of the ion drift is an additional energy loss, which reduces the overall efficiency of the excitation and dissociation processes.

The time duration of the ion phase is less than 1 μs. After this period the distribution of the surface charge density becomes practically symmetric (bipolar) and the charged region on the dielectric surface widens up to the far edges of the location of the electrodes. Both components of the field strength on the surface become zero between the location of the electrodes, and the cathode layer disappears (figure 9). A field strength reduction takes place not only on the dielectric surface but in the gas region up to about 70–100 μm above the surface as well.

The ion drift ceases after about half a microsecond. Part of the ions reach the dielectric surface, and part of them are left in the discharge volume. The discharge volume is now practically neutral and the density of the ions of both polarities is about $10^{14}\,\mathrm{cm}^{-3}$. The ions cannot drift because of the drastically reduced field strength and can only be neutralized by recombination. The known literature values of the recombination rate coefficients are scattered. The characteristic time of ion recombination is between 50 and 700 ns. After this period the discharge region becomes free of charged particles and the field strength is zero (the surface charge compensates the external voltage). If ignition conditions are reached again in the gas space, e.g. on account

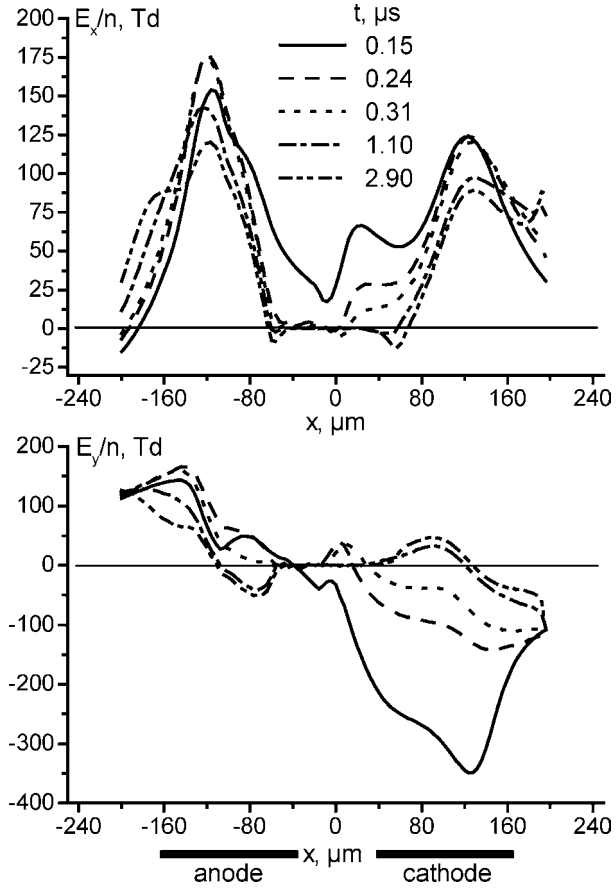

Figure 9. Temporal development of the field strength components on the dielectric surface during the ion phase of the discharge.

of a voltage rise or polarity change the next discharge pulse will happen.

3.4. Discharge current

In general the discharge current can be measured at any point of the electrical circuit. Per definition, current is the change of charge, e.g. at the electrodes of the discharge system. This value can be found for the V = const approach as described in section 2.2. In the Q = const case no current flows in the external circuit, although the discharge happens (as a result of the energy accumulated in the capacity of the electrode system). In this case the effective current is defined by the flux of charge carriers in the gas region. It can be calculated according to the Sato–Morrow equation [28] (which approximately means division of the discharge power by the applied voltage).

In the V = const case the discharge current calculated using the approach described in section 2.2 is identical to that obtained using the Sato–Morrow equation. In figure 10 the simulated current pulse shapes for both cases are given.

The current shapes consist of a steep rise and a comparably slow decrease. The current rise is determined by the velocity of the cathode layer extension on the dielectric surface (figures 5 and 6). The current density in the cathode layer is constant during this process. The same phenomenon has been found in DBD arrangements with a gas gap between the electrodes [26].

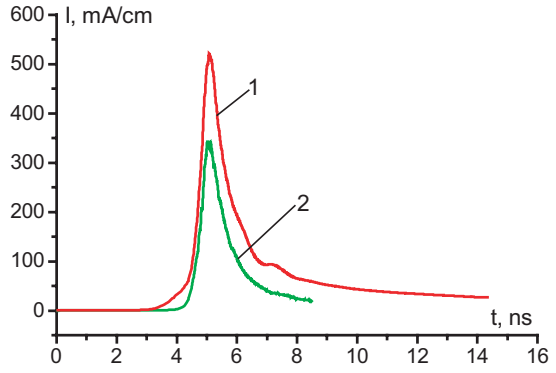

Figure 10. Current pulse in a CD-arrangement calculated with $V = \text{const}$ (external current, curve 1) and with $Q = \text{const}$ (effective current, curve 2).

The discharge duration (photo-emission included) is comparatively short, about 2–4 ns (figure 10). This value is several times shorter than measured ones in arrangements with a gas gap [29] (with different experimental conditions like the discharge gap and capacitance of the dielectric). The current shape is only slightly influenced by the external circuit. In the $V = \text{const}$ case it is a bit wider and its amplitude is about 40% higher than in the $Q = \text{const}$ case.

4. Energy release and efficiency

4.1. Energy release in the discharge volume

Energy release starts with the current flow and practically stops when the charged particle density in the discharge region decreases significantly. The energy release is determined by the drift of electrons and ions. The energy release connected with the electron drift happens mainly during the current pulse. The drift of ions becomes important later on.

The energy density, w, can be described by the time integral of the sum of scalar multiplications of the local field strength and the drift velocity of all charged particles (equation (5)),

$$w = e_0 \int \left(\sum |(\vec{E} \cdot \vec{v}_i)| \cdot n_i \right) \mathrm{d}t, \tag{5}$$

e_0 is the elementary charge, and the other parameters are as equations (1)–(4). Each charged particle (electrons, ions of both polarity) contributes to the energy consumption.

The first traces of energy release appear with the streamer development near the anode (left electrode in figure 11). A region with a significant energy density is found behind the cathode-directed streamer in the highly conductive channel, which grows and widens with the movement of the streamer head (cf figure 5 with figure 11). The position of the energy density maximum rises up to a height of 20 μm above the surface during this process. The mean value of the energy density in the discharge channel is about 15 mJ cm^{-3}. After the current maximum a second important region of energy release appears near the cathode (figure 11, $t = 9.9$ ns).

Part of the energy in the discharge region may be utilized for application purposes. For example, excitation of internal states of xenon is used in PDPs, dissociation of poisonous gases

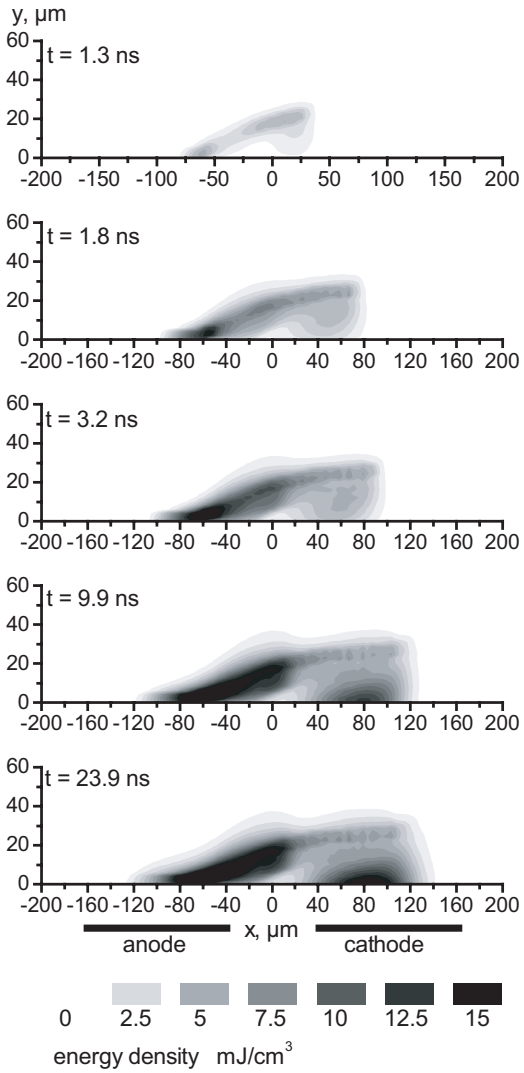

Figure 11. Temporal development of the energy density distribution in the discharge region.

is applied for gas cleaning purposes and molecular oxygen is used for ozone production. These processes happen during the electron phase of the discharge, when the electron density is high. While electron collisions last for a few nanoseconds, the following processes, like chemical reactions, can take much more time.

In figure 12 the distribution of the atomic oxygen density is presented as an example. It is similar to the energy density distributions in figure 11, with a difference in the cathode region. In this region the energy release is caused by ion drift; the ions are not able to dissociate oxygen. The degree of dissociation reached by a single discharge pulse is comparatively high, about 0.05% (figure 12).

Looking a bit more in detail at this process, it is of interest to mention that most of the O-atoms are generated in the discharge channel. Although the O-atom production rate is highest in the streamer head, with a high field strength, the main O-atom yield is gained in the channel, where the electric field strength is relative low (below 100 Td, figure 6). The small spatial–temporal volume of the streamer head is the reason for this phenomenon.

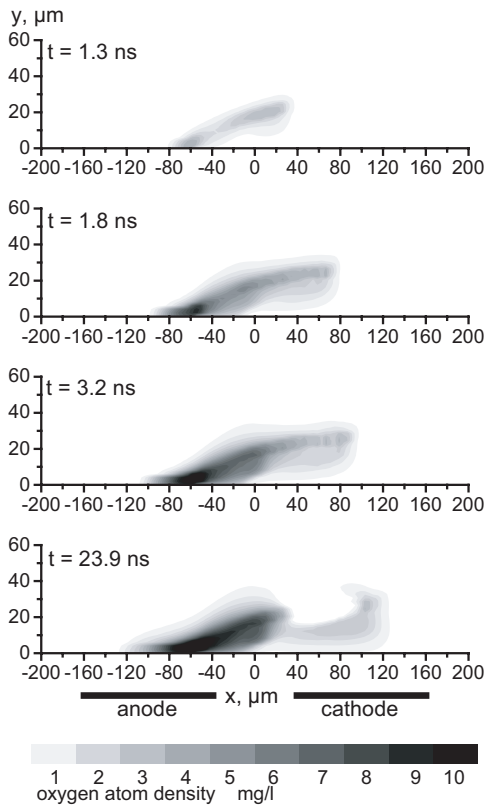

Figure 12. Temporal development of the O-atom density distribution in the discharge region.

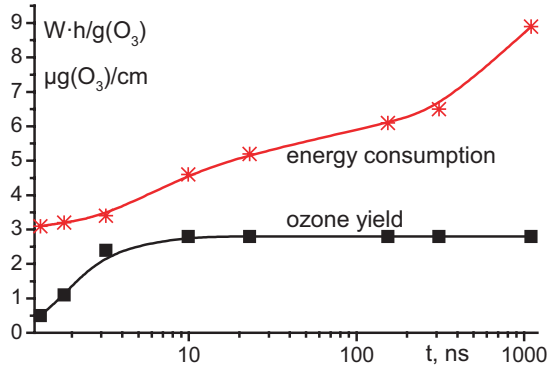

Figure 13. Specific energy consumption and ozone production per unit of electrode length during a discharge pulse in oxygen of 1.7 bar.

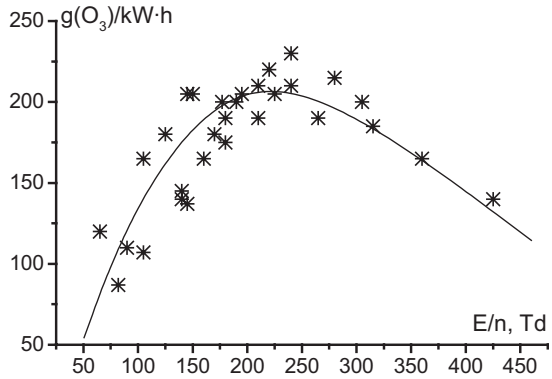

Figure 14. Measured values of the efficiency of ozone synthesis from oxygen [30].

4.2. Efficiency of electron collision processes

After the ion phase the energy transfer from the field to particles is completed, the final value of the energy consumption of the discharge pulse and the number of excited, ionized and dissociated particles are fixed. These values determine the efficiency of the process under consideration. In figure 13 an example of the reversal value of the efficiency (the specific energy consumption) is presented over the duration of the discharge pulse (the values are given for ozone molecules as all oxygen atoms are converted to ozone in this example).

The number of O-atoms rises during a discharge pulse up to the current maximum (at about 3.2 ns). During the ion phase, starting at about 10–15 ns, oxygen dissociation ceases, while the energy consumption continues. During the electron phase the energy consumption is lower because losses originating from ion drift are negligible. For example, for oxygen dissociation (i.e. ozone production), the specific energy consumption is close to the maximum theoretical value (of 3.2–4 W h g^{-1}, figure 13). However, after the ion phase the value rises up to about 9 W h g^{-1}, which is reached experimentally under optimum conditions.

The efficiency of ozone synthesis depends on the effective field strength (figure 14). The maximum of the efficiency (about 225 g $(kW\,h)^{-1}$) is reached at about 200 Td. The initial field strength in CD arrangements is non-homogeneous, and its maximum value is higher than 200 Td (figure 4); however, the final value of the efficiency of ozone synthesis only corresponds to about 100 Td (compare figure 13 with figure 14).

The values given in figure 14 result from measurements performed with a non-self-sustaining discharge. At a low gas pressure (40 Torr) electrons were produced by short UV pulses. The experimental conditions correspond to the left branch of the Paschen curve, so that high E/n values could be realized without breakdown. Under such a condition the charged particle density is too low to distort the homogeneous field distribution significantly, and oxygen dissociation takes place in a nearly constant field. A relatively high repetition frequency of the UV radiation pulses (1 kHz) and a steady gas glow ensure a reasonable accuracy of the data given in figure 14 [31].

The parameters of the external circuit influence the discharge dynamics and, in particular, the energy dissipation and transformation to excitation and dissociation processes. Considering the V = const and Q = const cases (section 2.2), some discharge parameters differ. In table 1 the values of energy, the transferred charge (both per centimetre of electrode length) and the specific energy consumption of O_3 generation are presented for three time stages of the discharge development.

The current pulse duration of the electron phase is about 4–6 ns in both cases. In the V = const case the value of the transferred charge, as well as the energy consumption, is higher than in the Q = const case. From this follows a voltage drop; in the Q = const case this happens earlier and the energy consumption is 15–20% lower. (The transferred charge for Q = const is determined by the multiplication of the voltage drop at the electrodes and the capacity of the device.)

Table 1. Values of the discharge parameters for the V = const and Q = const (oxygen of 1.7 bar) cases.

	V = const			Q = const		
Time, ns	7.5	122	536	8.0	129	544
Energy, μJ cm^{-1}	1.67	2.60	2.96	1.06	1.71	2.00
Transferred charge, nC cm^{-1}	0.68	1.38	1.56	0.56	0.90	1.05
Specific energy consumption, W h g^{-1} O_3	6.6	10.3	11.8	5.4	8.7	10.0

5. Discussion

5.1. Current pulse and photoemission

The duration of the current pulses is only a few nanoseconds (figure 10). This order of magnitude has been found experimentally in DBDs in oxygen and air as well [32, 33]. The current pulse duration decreases from about a hundred to a few nanoseconds if photo-stimulated processes are included in the modelling. Two principal sources of additional electrons exist, photo-stimulated processes (photo-emission on surfaces and photo-ionization in the gas volume) and surface emission caused by the impact of positive ions on surfaces. If only the latter is considered, the rise time of the current pulse is about 100 ns, and its amplitude about 10 mA [16–18], in contrast with some experimental results [34–39].

Photo-ionization is considered to be the principal (and only) mechanism of streamer formation and propagation [40–43]. Photo-ionization in the gas region needs UV photons of more than 10 eV. Photo-emission from surfaces requires photon energies of only 4–6 eV. If photo-emission is not included in the model, i.e. the only source of secondary electrons is ion impact, streamers do not appear. In this case the current pulse duration is rather long, and its amplitude is some orders of magnitude smaller than with considering photo-emission [26, 37, 39].

By modelling, it has been discovered that the ozone yield (production and efficiency) is independent of photo-emission. This can be explained as follows: ozone is mainly produced in the conductive region of the discharge. The mean field strength in the channel, determined by the equilibrium between electron production and losses, depends on the gas properties and is not affected by the photo-emission process on surfaces. The electron density is lower if photo-emission is not included in the model; however, the discharge duration is increased. As a result of this, the ozone yield is comparable in both cases, although the dynamics of the initial phase of the breakdown process is far from being real without photo-emission [29].

5.2. Poisson equation and boundary conditions

The thickness of the discharge region in CD arrangements is about 20–30 μm at around atmospheric pressure. The main processes, such as the streamer movement and charge accumulation, happen in a thin layer on the surface. Hence an accurate determination of the field distribution on the dielectric surface and in a thin layer above is of crucial importance for the simulation of CDs.

The correct mathematical formulation of the problem is as follows: there are two regions of different permittivity (dielectric and gas region). In each region the Poisson equation must be solved separately. To connect the two regions the well-known relations for the tangential and normal components of the field strength must be applied on the boundary of the dielectric. As the boundary between the two regions is a surface (with no thickness), the Poisson equation is not valid here.

The technical realization of such a situation is difficult. Usually, regions with different permittivity are united to a continuous one with varying permittivity [11–14, 16–22, 44–48]. In this case the real permittivity jump at the dielectric surface is substituted by a continuous function in a certain layer replacing the surface. These approaches work well if the most important processes take place far from the dielectric boundary. In CD arrangements the main processes, however, happen just on the dielectric surface.

The field distributions directly on the dielectric surface differ considerably with the two approaches. The value on the dielectric surface is about two times smaller than the accurate one if the continuous change in the permittivity (cell size 2 μm) is considered. In this case the discharge develops comparatively slowly, and the duration of the current pulse increases.

In order to get the correct field strength distribution, accurate potential values on the boundaries (including the dielectric surface) are necessary. For this purpose the image charge method was used [7, 26]. The charge distributions in the discharge region, on the dielectric surface and on the conductive electrodes were taken into account. The field strength in the gas region was determined using common differential methods.

This approach describes the processes near and on the dielectric surface accurately. An additional advantage of this procedure is the ability to determine the potential at any boundary correctly. With correct potential values on the boundaries the integration region can be reduced considerably.

5.3. Implicit and explicit method

The explicit algorithm used to describe the dynamics of charged particles has the known disadvantage of needing a high numbers of time steps (*Courant* limitation) [11, 20].

The implicit approach can be used with relatively large time intervals, i.e. a smaller number of time steps. It is reported that the time interval can be increased up to several nanoseconds under ambient conditions [11, 20]. Under these conditions electrons drift about 200 μm in 1 ns at breakdown field strength; this is why the spatial resolution is less than 200 μm with a 1 ns time step and phenomena like formation of a cathode layer and streamers cannot be resolved. Time intervals of 20 ps or less are necessary to describe these structures with a size of about 20 μm at atmospheric pressure. With 20 ps time steps the implicit algorithm loses its advantage.

The implicit algorithm (with large time steps) is preferentially applicable to relatively slow developing processes and low spatial resolutions. If it is applied to fast processes some doubts appear whether the spatial–temporal resolution is sufficient to resolve detailed structures of the discharge.

6. Conclusions

DBDs in CD arrangements consist of a multitude of discharge channels that develop in the gas space along the surface. The dynamic behaviour has been modelled on a two-dimensional approach. The formation of channels starts with cathode- and less pronounced anode-directed streamers, which move from the inner edges of the electrodes to the outer ones on the surface. The movement of the cathode-directed streamer is followed by the development and extension of a cathode layer. The cathode layer is a source of secondary electrons that supports the development of a conductive channel between the streamer heads.

It has been found that photo-emission must be considered in order to describe the current pulse duration of a few nanoseconds at atmospheric pressure correctly. The charge transfer through the channel and its accumulation on the surface cause a decay of the channel. The dynamics of the discharge development in CD arrangements is similar to those in other DBD arrangements.

In electronegative gases (oxygen) the mean electric field strength in the discharge channels is high enough to excite particles and/or produce radicals. The streamer area is of less importance. The efficiency of these processes is determined by electron collisions in the electron phase of the discharge. Later on, during the extinction and ion phases, it is reduced by the energy consumption of the ion drift. The simulated overall efficiency values conform to measured ones.

For modelling the discharge in CD arrangements the accuracy of the field determination near and on the dielectric surface has a crucial effect on the breakdown process. Depending on the numerical approach, a cathode-directed streamer does or does not appear, and the duration of the discharge varies considerably.

Acknowledgments

The investigations were carried out mainly in the frame of a cooperation with Toshiba Corp., Japan. The authors wish to express thanks to Dr. Takaii Murata and his colleagues for their contribution. Part of the investigations has been supported by the International Bureau of the Federal Ministry of Education and Research of Germany.

References

[1] Hulka L and Pietsch G J 2002 On the ignition voltage and structure of coplanar barrier discharges *Contributed Papers: Int. Symp. on High Pressure, Low Temp. Plasma Chemistry (HAKONE VIII) (Pühajärve, Estonia)* vol II, pp 259–63

[2] Murata T, Okita Y and Terai K 1997 Distribution of surface discharge for ozone generation *Proc. 23rd Int.Conf. on Phenomena in Ionized Gases (Toulouse)* vol III, pp 82–3

[3] Murata T, Okita Y, Noguchi M and Takase I 2001 Basic parameters of coplanar discharge ozonizer *Proc. 15th World Congress of the Int. Ozone Association (London)* vol III, pp 39–54

[4] Okita Y, Iijima T, Amano A, Yamanashi I and Murata T 2003 Development of compact 1 kg h^{-1} coplanar discharge ozonizer *IEE J. Trans. FM (Fundamentals and Materials)* **123** 39–54 (in Japanese)

[5] Savel'ev A B, Gibalov V I, Pietsch G J and Saenko V B 1999 Efficiency of ozone synthesis in surface discharge arrangements *Proc. 14th Int. Symp. on Plasma Chemistry (Prague)* vol V, pp 2343–8

[6] Gibalov V I, Murata T and Pietsch G J 2000 Modelling of the discharge development in coplanar arrangements *Proc. 13th Int. Conf. on Gas Discharges and their Applications (Glasgow)* vol I, pp 275–8

[7] Gibalov V I, Murata T and Pietsch G J 2001 Productivity and efficiency of ozone synthesis in coplanar discharge arrangements *Proc. 15th World Congress of the Int. Ozone Association (London)* vol III, pp 1–14

[8] Gibalov V I, Murata T and Pietsch G J 2001 Discharge dynamics and ozone synthesis in coplanar barrier discharge arrangements *Proc. 15th Int. Symp. on Plasma Chemistry (Orléans)* vol II, pp 437–42

[9] Gibalov V I, Murata T and Pietsch G J 2002 Some characteristic parameters of coplanar discharge arrangements *Proc. 14th Int. Conf. on Gas Discharges and their Applications (Liverpool)* vol I, pp 183–6

[10] Gibalov V I and Pietsch G J 2004 Properties of dielectric barrier discharges in extended coplanar electrode systems *J. Phys. D: Appl. Phys.* **XX** yy–zz

[11] Rauf S and Kushner M 1999 Dynamics of coplanar-electrode plasma display panel cell I. Basic operation *J. Appl. Phys.* **85** 3460–9

[12] Rauf S and Kushner M 1999 Dynamics of coplanar-electrode plasma display panel cell II. Cell optimization *J. Appl. Phys.* **85** 3470–6

[13] Rauf S and Kushner M J 1999 Operation of a coplanar-electrode plasma discharge panel cell *IEEE Trans. Plasma Sci.* **27** 10–11

[14] Boeuf J P, Punset C, Hirech A and Doyeux H 1997 Physics and modeling of plasma display panels *J. Phys. IV* **C4** 3–14

[15] Guo J-M 1993 Two-Dimensional nonequilibrium fluid model for streamers *IEEE Trans. Plasma Sci.* **21** 684–95

[16] Cambell R B, Veerasingam R and McGrath R T 1995 A two-dimensional multispecies fluid model of plasma in an AC plasma display panel *IEEE Trans. Plasma Sci.* **23** 698–708

[17] Pashaie B, Sankaranarayanan R and Dhali S K 1999 Experimental investigation of microdischarges in a dielectric-barrier discharge *IEEE Trans. Plasma Sci.* **27** 22–3

[18] Ventzek P L G, Sommerer T J, Hoekstra R J and Kushner M J 1993 Two-dimensional hybrid model of inductively coupled plasma sources for etching *Appl. Phys. Lett.* **63** 605–7

[19] Punset C, Cany S and Boeuf J P 1999 Addressing and sustaining in alternating current coplanar plasma display panels *J. Appl. Phys.* **86** 124–33

[20] Fiala A, Pitchford L C and Boeuf J P 1994 Two-dimensional hybrid model of low-pressure glow discharge *Phys. Rev.* E **49** 5607–22

[21] Punset C, Boeuf J P and Pitchford L C 1998 Two-dimensional simulation of an alternating current matrix plasma display cell: cross-talk and other geometric effects *J. Appl. Phys.* **83** 1884–97

[22] Cho T-S, Ko J-J, Kim Dae-Il, Lee C-W, Cho G and Choi E-H 2000 Influence of sustaining pulse-width on electro-luminous efficiency in AC plasma display panels *Japan. J. Appl. Phys.* **39** 4176–80

[23] Book D L, Boris J P and Hain K 1975 Flux-corrected transport II, generalizations of the method *J. Comput. Phys.* **20** 248–83

[24] Georghiou G E, Morrow R and Metaxas A C 1999 An improved finite element flux-corrected transport algorithm *J. Comput. Phys.* **148** 605–20

[25] Georghiou G E, Morrow R and Metaxas A C 2000 A two-dimensional, finite element, flux-corrected transport

algorithm for solution of gas discharge problems *J. Phys. D: Appl. Phys.* **33** 2453–66
[26] Gibalov V I and Pietsch G J 2000 The development of dielectric barrier discharge in gas gaps and on surfaces *J. Phys. D: Appl. Phys.* **33** 2618–36
[27] Eliasson B and Kogelschatz U 1986 Basic data for modelling of electric discharges in gases: oxygen *Brown Boveri Research Report* KLR 86-11 C
[28] Morrow R and Sato N 1999 The discharge current induced by the motion of charged particles in time-dependent electric fields; Sato's equation extended *J. Phys. D: Appl. Phys.* **32** L20–2
[29] Küchler U and Pietsch G 1992 Current mesurement of microdischarges in ozonizers *Proc. 10th Int. Conf. on Gas Discharges and their Applications (Swansea)* pp 506–9
[30] Gibalov V I 1994 Synthesis of ozone in a barrier discharge *Russ. J. Phys. Chem.* **68** 1029–33
[31] Pravdin A B and Gibalov V I 1989 Ozone synthesis with non-self sustaining discharge *J. Phys. Chem. (Russ.)* **LXIII** 2785–9
[32] Heuser C and Pietsch G 1980 Prebreakdown phenomena between glass-glass and glass-metal electrodes *6th Int. Conf. on Gas Discharges and their Applications (Edinburgh) IEE Conf. Publ.* vol 189, pp 98–101
[33] Hirth M 1981 Teilprozesse bei der Ozonerzeugung mittels stiller elektrischer Entladungen, Teil I: Die elektrische Entladung im Ozonisator, Teil II: Die Ozon- und Stickoxydbildung im Ozonisator *Beitr. Plasmaphys.* **20** 1–27
[34] Adler F and Müller S 1998 Temporally and spatially resolved spectroscopic investigation of dielectric barrier discharges *Proc. Science and Technology of Light Sources (LS16) (Greiswald)* pp 376–7
[35] Gottschalk J R, Shvydky O, Compaan A D, Theodosiou C E and Williamson W 1999 Time-resolved electrical and optical measurements in a plasma display panel *IEEE Trans. Plasma Sci.* **27** 772–7
[36] Callegari Th, Ganter R and Boeuf J P 2000 Diagnostic and modeling of a macroscopic plasma display panel cell *J. Appl. Phys.* **88** 3905–13
[37] Braun D, Gibalov V and Pietsch G 1992 Two-dimensional modelling of the dielectric barrier discharge in air *Plasma Sources Sci. Technol.* **1** 1–23
[38] Georghiou G E, Morrow R and Metaxas A C 2001 The effect of photoemision on the streamer development and propagation in short uniform gaps *J. Phys. D: Appl. Phys.* **34** 200–8
[39] Akishev Y S, Grushin M E, Deryugin A A, Napartovich A P, Pankin M V and Trushkin N I 1999 Self-oscillations of a positive corona in nitrogen *J. Phys. D: Appl. Phys.* **32** 2399–409
[40] Babaeva N Y and Naidis G V 1996 Two-dimensional modelling of positive streamer dynamics in non-uniform electric fields in air *J. Phys. D: Appl. Phys.* **29** 2423–31
[41] Morrow R and Blackburn T R 1999 The role of photoionization in streamer discharge formation in voids *IEEE Trans. Plasma Sci.* **27** 26–7
[42] Kulikovsky A A 2000 The role of photoionization in positive streamer dynamics *J. Phys. D: Appl. Phys.* **33** 1514–24
[43] Pancheshnyi S V, Starikovskaia S M and Starikovskii A Y 2001 Role of photoionization processes in propagation of cathode-directed streamer *J. Phys. D: Appl. Phys.* **34** 105–15
[44] Xu X "Peter" and Kushner M J 1999 The consequences of remnant surface charges on microdischarge spreading in dielectric barrier discharges *IEEE Trans. Plasma Sci.* **27** 108–9
[45] Muller I, Punset C, Ammelt E, Purwins H-G and Boeuf J P 1999 Self-organized filaments in dielectric barrier glow *IEEE Trans. Plasma Sci.* **27** 20–1
[46] Shin Y K, Lee J K and Shon C H 1999 Two-dimensional breakdown characteristics of PDP cells for varying geometry *IEEE Trans. Plasma Sci.* **27** 14–5
[47] Jeong H S, Shin B-J and Whang K-W 1999 Two-dimensional multifluid modeling of He-Xe discharge in an AC plasma display panel *IEEE Trans. Plasma Sci.* **27** 171–81
[48] Al-Hussany A and Davies A J 1997 A stable high resolution scheme for discharge simulation *Contributed Papers: 23rd Int. Conf. on Phenomena in Ionized Gases (ICPIG XXIII) (Toulouse)* vol II, pp 218–19